Journal of the Korean Physical Society, Vol. 77, No. 6, September 2020, pp. 515∼523

Improvement with the Multi-material Decomposition Framework in Dual-energy Computed Tomography: A Phantom Study

Haenghwa Lee
Department of Radiological Science, Department of Radiological Sciences, Yonsei University, Wonju 26493, Korea

Hee-Joung Kim*
Department of Radiological Science, Department of Radiological Sciences, Yonsei University, Wonju 26493, Korea and Department of Radiation Convergence Engineering, Department of Radiological Sciences, Yonsei University, Wonju 26493, Korea

Donghoon Lee, Dohyeon Kim, Seungyeon Choi and Minjae Lee
Department of Radiation Convergence Engineering, Department of Radiological Sciences, Yonsei University, Wonju 26493, Korea

(Received 22 May 2020; revised 9 June 2020; accepted 6 July 2020)

Dual energy computed tomography (DECT) enhances tissue characterization by obtaining two or three material images from two measurements with different X-ray spectra. Recently, multi-material decomposition (MMD) in DECT has been studied to obtain decomposed material images for more than three basis materials. However, the MMD method is highly sensitive to noise fluctuation due to the direct inversion and the material triplet selection for each pixel. Although several studies have reported to reduce the noise resulting from direct inversion, no studies have researched reduction in the image quality degradation caused by material triplet selection. We proposed a MMD framework for DECT that includes pre-decomposition and post-decomposition stages to reduce image quality degradation due to material triplet selection and direct inversion. The total variation denoising method was applied to the pre-decomposition and the post-decomposition stages as a noise suppression algorithm. The digital phantom, tissue characterization phantom, and Catphan phantom were employed as test objects in this study. The volume fraction accuracy (VFA) and the standard deviation (STD) were quantitatively calculated to evaluate the quality of the decomposed images. The results of the proposed method were compared to those of the direct MMD (DMMD) and the MMD with total variation denoising (MMD-TVD) methods. Compared to the DMMD method, the proposed method improved average the VFA value by 11.40%, 17.31%, and 19.13% in the digital phantom, the tissue characterization phantom, and the Catphan phantom studies, respectively. The STD values for the proposed method are better than those of the DMMD method, and are similar to those of the MMD-TVD method. Our method successfully improved quantification accuracy and suppressed noise. In conclusion, the proposed method resulted in quantitatively better multi-material images for DECT.

Keywords: Multi-material decomposition, Dual-energy computed tomography, Material triplet library
DOI: 10.3938/jkps.77.515

I. INTRODUCTION

Dual-energy computed tomography (DECT) has been used to reconstruct commonly two or three basis materials with additional measurement information. Dual tubes with or without beam filtration, rapid voltage switching, dual-layer detector, split filter technique, and sequential scanning are currently available systems for DECT [1–3]. The major advantage of DECT is the material characterization and quantification due to its capability of material discrimination. DECT is now widely used in clinics for virtual mono-energetic imaging, automated bone removal in CT angiography, perfused blood volume measurements, virtual non-contrast imaging, urinary calcification detection, atherosclerotic plaque removal, *etc.* [4].

Typically, material decomposition methods can distinguish only two substances or up to three substances [3]. However, some clinical applications require three or more decomposed images. For example, urinary calcification detection requires discrimination of various stone

*E-mail: hjk1@yonsei.ac.kr, cohost20@yonsei.ac.kr

 ©2020 The Korean Physical Society

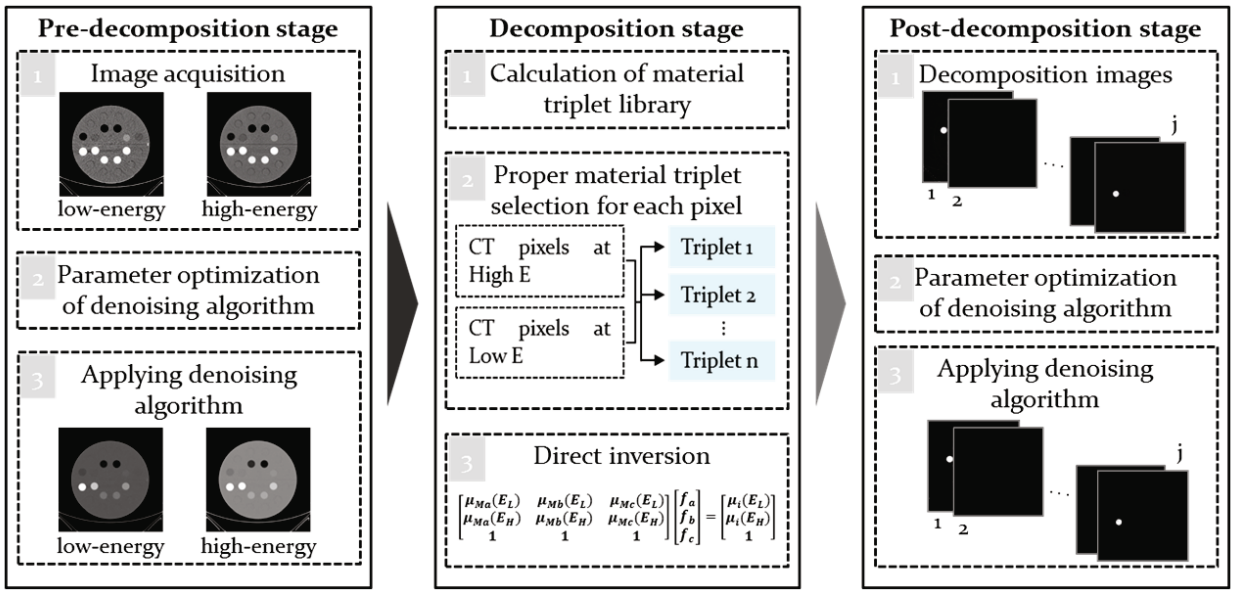

Fig. 1. Block diagram of the proposed MMD framework.

types, such as brushite ($CaHPO_4{\cdot}2H_2O$), calcium oxalate (CaC_2O_4), struvite ($(NH_4)MgPO_4{\cdot}6H_2O$), cysteine ($C_6H_{12}N_2O_4S_2$), and uric acid ($C_5H_4N_4O_3$) [5, 6], because the causes and the treatments of stone types are different [7]. In liver-fat quantification, quantification of liver tissue, fat, blood, and contrast agents are needed simultaneously.

One of the special DECT clinical applications is multi-material decomposition (MMD), which identifies various basis materials by using the extended concept of three-material decomposition. There are several MMD methods to provide images of multiple basis materials. They can be divided into three categories: the projection-domain, the one-step inversion, and the image-domain methods [8]. Projection-domain methods convert two measurements into sinograms for the various basis materials and then reconstruct basis material images by using a conventional reconstruction algorithm. These methods remove beam-hardening artifacts due to the estimated material basis projections before reconstruction [9]. However, one challenge is that the decomposition accuracy is limited by the calibration accuracy. One-step inversion methods acquire multiple basis-material images from the projection data by using simultaneous image reconstruction and material decomposition. For example, Long and Fessler [10] proposed the one-step inversion MMD method based on penalized-likelihood (PL) reconstruction. This method decreased noise by the exact modeling of the physics of spectral transmission. Nevertheless, it is computationally expensive due to repeated projections and back-projections during the MMD and reconstruction process. Image-domain methods directly decompose the CT images into basis materials images. They are computationally efficient and more convenient compared to the projection-domain and the one-step inversion methods. For instance, Mendoca *et al.* [11] proposed a direct MMD (DMMD) method that calculates the volume fraction of the selected basis material after distributing pixels of the CT images to the appropriate material triplet. Although this method yielded quantitatively accurate results for virtual unenhancement and liver-fat quantification, it leads to magnified noise due to material triplet selection and direct inversion without considering the noise statistics of the CT images.

That noise is magnified due to direct inversion in DECT is well known. Xue *et al.* [12] proposed a statistical image-domain MMD method to reduce this noise. Their method estimates multiple material images from high- and low-energy CT images by using a penalized weighted least-squares (PWLS) method with edge-preserving (EP) regularization terms. Ding *et al.* [13] proposed a PWLS algorithm with three regularization terms, what is called PWLS-TNV-l_o. This method increased decomposition accuracy compared to the PWLS-EP method because it considers prior information and encourages sparsity of material composition in each pixel using regularization. The non-convex material sparsity penalty for the image-domain MMD method proposed by Lyu *et al.* [14] improved the volume fraction accuracy (VFA) and diagonal elements of the normalized cross correlation (NCC) matrix. These studies that apply the noise suppression algorithm before or after [12–16] decomposition for the image-domain MMD method have reported a reduction in the magnified noise caused by direct inversion. However, no studies have reported on the need to apply a noise suppression algorithm both before and after decomposition.

We proposed an MMD framework that consists of three steps: pre-decomposition, material decomposition, and post-decomposition. The proposed MMD frame-

work is discussed in detail in Sec. II. We used total variation denoising as a noise suppression algorithm because it preserves details as well as reduces noise [17]. The performance is evaluated using digital, Catphan700, and tissue characterization model 467 phantoms. The results of the proposed method were compared to the results of the DMMD [11] and MMD methods with total variation denoising (MMD-TVD).

II. MATERIALS AND METHODS

1. Proposed MMD Framework

The proposed MMD framework consisted of three steps: pre-decomposition, decomposition, and post-decomposition. The flowchart of proposed MMD framework is shown in Fig. 1. The pre-decomposition stage was used for the noise suppression algorithm to select the appropriate material triplet for each pixel in the decomposition stage. The decomposition stage used the DMMD [11] method because it is simply performed in the image domain as described in below. In this stage, the proper material triplet was calculated for each pixel; then, the volume fraction of the selected basis material was obtained. The post-decomposition stage reduced the noise of decomposed images resulting from direct inversion.

CT images contain not only quantum and anatomical noise but also noise resulting from the ramp filter. The obtained images can be represented as follows:

$$y = x + \omega \tag{1}$$

Here, the y value is a noise-corrupted image, the x value is the original image, and the ω value is noise. Material triplet selection in the decomposition stage without considering the noise can led to the choice of an improper material triplet for each pixel, thus magnifying the noise and decreasing the quality of image (Figure 2). For this reason, the reconstructed CT images need noise suppression in the pre-decomposition stage. Direct inversion in decomposition is well known to lead to noise magnification [12–18]. Therefore, the noise resulting from direct inversion in the post-decomposition stage needs to be reduced.

In both the pre- and the post-decomposition stages, total variation denoising [19] was used as a noise suppression algorithm. The total variation denosing model can be expressed as [17,19]

$$\underset{x}{\operatorname{argmin}} \frac{1}{2} \parallel y - x \parallel_2^2 + \lambda TV(x). \tag{2}$$

Here, the y value and the x value are the input image and the output image, respectively. In pre-decomposition stage, input images are noisy CT images at low- and high-energies. The input values in post-decomposition stage were material images. The regularization parameter, λ, controls the degree of smoothing. To determine a proper λ for all images in the pre- and the post- decomposition stages, we calculated the maximum VFA.

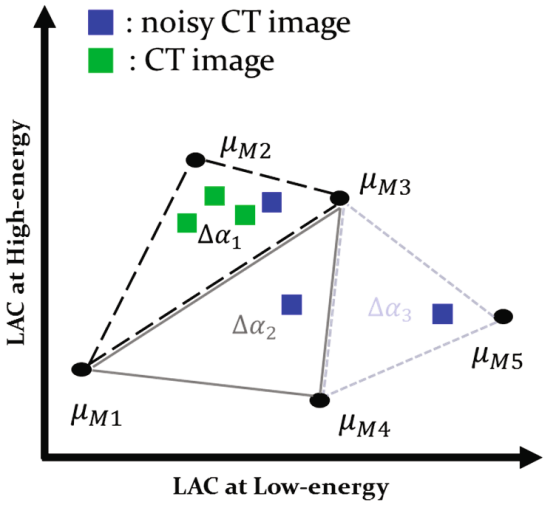

Fig. 2. Geometric interpretation of the material triplet selection step for each pixel with and without noise.

The decomposition stage assumes that similar constraints are applied in the DMMD method [11]. This method assumes that the volume and mass of the material fraction are conserved. This also assumes that each pixel contains up to three basis materials, and the type of basis materials for each pixel can be changed [11–13].

Before the decomposition stage, the information already obtained is CT images at low and high energy and known material compositions. The linear attenuation coefficient (LAC) pair of CT images at low- and high-energies can be expressed as follows:

$$\mu_i = (\mu_i(E_L), \mu_i(E_H)), \tag{3}$$

where $\mu_i(E_L)$ and $\mu_i(E_H)$ mean the i-th pixel values of the CT image at low- and high-energies, respectively. We calculated the LAC pairs of known material compositions at low- and high-energies by using:

$$\mu_{Mj} = (\mu_{Mj}(E_L), \mu_{Mj}(E_H)), \tag{4}$$

where $\mu_{Mj}(E_L)$and $\mu_{Mj}(E_H)$ are the LAC value of the j-th basis material at low- and high-energies, respectively.

In the decomposition stage, we first generated a material triplet library. The material triplet library should include all possible triplets from LAC pairs μ_{Mj} of the selected basis materials and avoid intersection between material triplets [11]. An adequate material triplet library was selected using the Delaunay triangulation method [20]. This method is easy to implement and prevents the intersection between material triplets. Secondly, this method selected the proper material triplet for each pixel. When pixel (μ_i) does not fall inside or at the

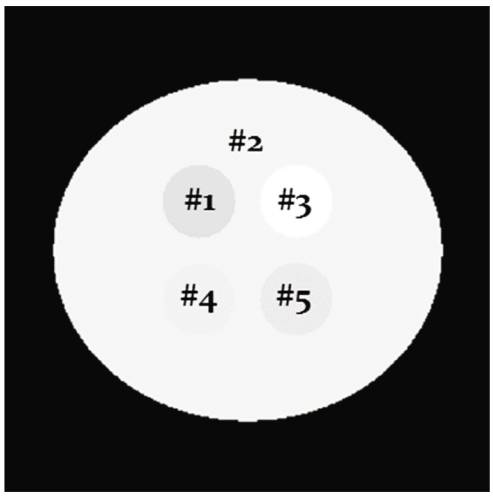

Fig. 3. Reconstructed image of the digital phantom.

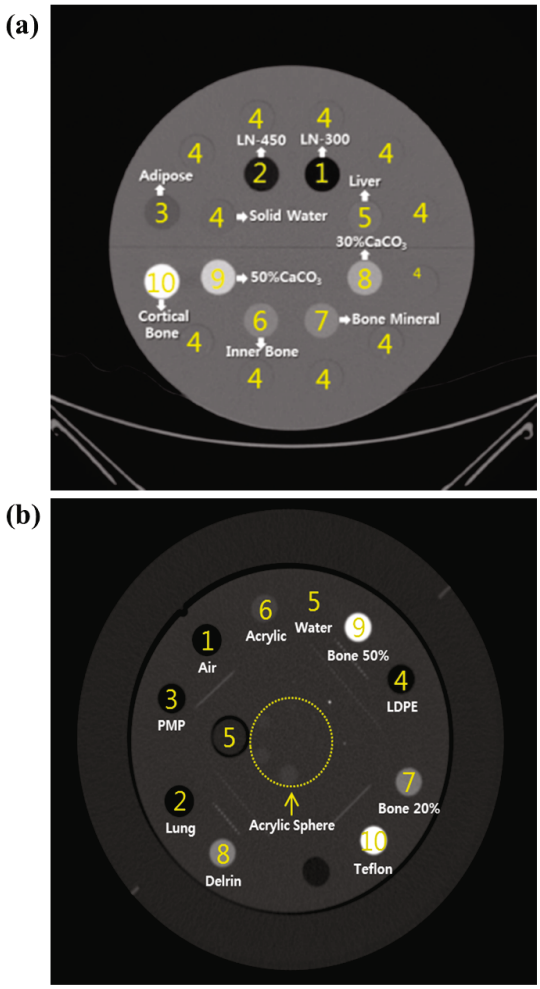

Fig. 4. Reconstructed images of (a) the tissue characterization Model 467 phantom and (b) the CTP 682 module phantom.

Table 1. Concentration ratios of the basis materials in the digital phantom.

Number	Material	Ratio
1	Adipose	1
2	Water	1
3	Blood	1
4	Water-Adipose	0.8:0.2
5	Water-Adipose	0.5:0.5

boundary of any triplet, the triplet with a minimal Hausdorff distance to pixel μ_i is selected as the solution [11]. Lastly, we decomposed each pixel (μ_i) into the volume fraction of basis materials that correspond to the proper material triplet. The volume fractions of the three basis materials for each pixel (μ_i) via direct matrix inversion can be calculated as (Ax = B) [21]:

$$\begin{pmatrix} \mu_{Ma}(E_L) & \mu_{Mb}(E_L) & \mu_{Mc}(E_L) \\ \mu_{Ma}(E_H) & \mu_{Mb}(E_H) & \mu_{Mc}(E_H) \\ 1 & 1 & 1 \end{pmatrix} \begin{bmatrix} f_a \\ f_b \\ f_c \end{bmatrix} = \begin{pmatrix} \mu_i(E_L) \\ \mu_i(E_H) \\ 1 \end{pmatrix}. \quad \{a,b,c\} \in \bigcup j \tag{5}$$

The first term A is the proper triplet ($\Delta\alpha_k$) of the material triplet for each pixel (μ_i). The second term x is the volume fractions of the three basis materials. The elements in x satisfy mass and volume conservation ($f_a+f_b+f_c = 1$). The third term means the LAC pairs of images. The solution of Eq. (4) can give the barycentric coordinates of the pixel (μ_i) with respect to the triangle ($\Delta\alpha_k$) [11]. In the MMD-TVD and the proposed methods, the decomposition stage used the DMMD [11–13] method.

2. Simulation Setup

The proposed method was evaluated using the digital phantom. The LAC values in the digital phantom were obtained from the National Institute of Standards and Technology (NIST) database [22]. We generated CT measurements at 80- and 140- kVp spectra provided by Spektr 3.0 [23]. The source-to-detector distance (SDD) was 1500 mm, and the source-to-object distance (SOD) was 1100 mm. Poisson noise was added to the simulated projection images. The filtered back-projection (FBP) algorithm was applied to reconstruct high- and low-energy CT images. We used adipose, water, blood, and air as the basis materials to construct the digital phantom as shown Fig. 3 and Table 1. To evaluate the

Table 2. Physical density of 10 basis materials for the tissue characterization Model 467 phantom and the CTP 682 module phantom.

Number	Basis materials set1 (Tissue characterization phantom)		Basis materials set2 (CTP 682 module phantom)	
	Basis materials	Physical Density	Basis materials	Physical Density
1	LN-300	0.30	Air	0.01
2	LN-450	0.45	Lung	0.17
3	Adipose	0.94	PMP	0.85
4	Solid Water	1.02	LDPE	0.95
5	Liver	1.10	Water	1.00
6	Inner Bone	1.14	Acrylic	1.15
7	Bone Mineral	1.15	Bone 20%	1.08
8	30% $CaCO_3$	1.34	Delrin	1.33
9	50% $CaCO_3$	1.56	Bone 50%	1.31
10	Cortical Bone	1.82	Teflon	1.87

decomposition capability of the proposed method on material mixtures, we used the basis materials to synthesize material mixtures with different concentration ratios.

3. Experimental Setup

We used a Brilliance 64-slice multi-detector computed tomography (MDCT) scanner (Philips, Eindhiven, The Netherlands) in Wonju Sevrance Christian Hospital (Wonju, Korea). The Brilliance 64 CT scanners consist of an MRC X-ray tube and NanoPanel tile detectors. The images were acquired at 80 and 140 kVp. The high- and low-energy CT images were reconstructed using the FBP algorithm. The SDD was 1040 mm, and the SOD was 570 mm. The matrix size of each reconstructed image was 512 × 512 with a pixel pitch of 0.78 mm.

Two phantoms were employed as the test objects in this study (Figure 4). One is the tissue characterization Model 467 (Gammex Inc, Middleton, WI, USA) phantom. The other phantom was the CTP 682 module contained in the Catphan 700 (The Phantom Laboratory Inc., Salem, NY, USA) phantom. Table 2 shows the physical densities of the 10 selected basis materials in the two phantoms.

4. Performance Evaluation

To quantify the evaluation of the material decomposition accuracy, we calculated the values of the VFA for all material images. The VFA of materials in the region of interest (ROI) is defined as [12,13],

$$\mathrm{VFA} = \left(1 - \frac{1}{L_0}\sum_{l=1}^{L_0}\frac{\bar{x_j}^{\mathrm{truth}} - \bar{x_j}}{\bar{x_j}^{\mathrm{truth}}}\right) \times 100\%. \quad (6)$$

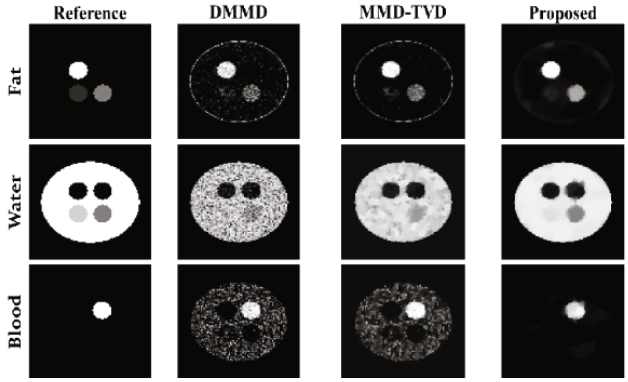

Fig. 5. Decomposed images of the digital phantom with noise using the DMMD (2nd column), the MMD-TVD (3rd column), and the proposed (4th column) methods. The first column is the ground truth of the material images. The rows from top to bottom are the decomposed fat (the 1st row), water (2nd row), and blood (3rd row) images.

Here, $\bar{x_j}^{\mathrm{truth}}$ is true ground value. The $\bar{x_j}$ value is the mean value of the ROI for the j-th material image. L_0 is total number of basis materials. The mean $\bar{x_j}$ of the j-th material image is defined as:

$$\bar{x_j} \triangleq \frac{\sum_{j=1}^{M} x_{lj}}{M}. \quad (7)$$

The STD measures the standard deviation of the specific ROI for the j-th material images. Noise reduction is successfully implemented when the STD is lower, where STD is defined as follows [12,13]:

$$\mathrm{STD} = \sqrt{\frac{1}{M}\sum_{j=1}^{M} x_{lj} - \bar{x_j}^2}, \quad (8)$$

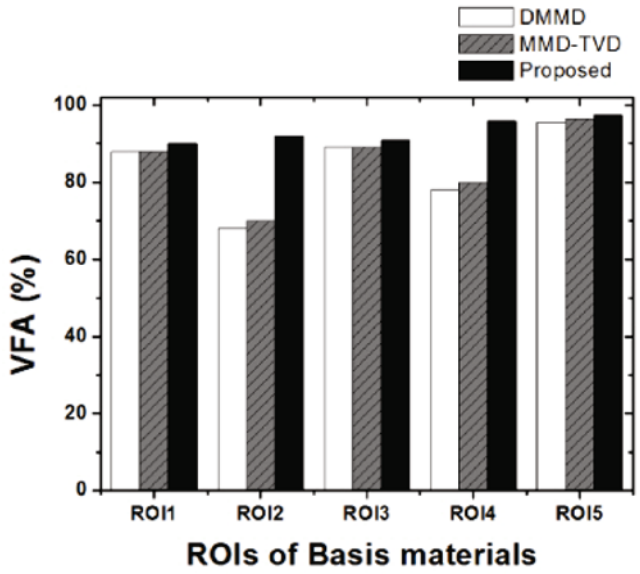

Fig. 6. VFA values of five ROIs for the digital phantom as obtained using the DMMD (white), the MMD-TVD (gray), and the proposed (black) methods.

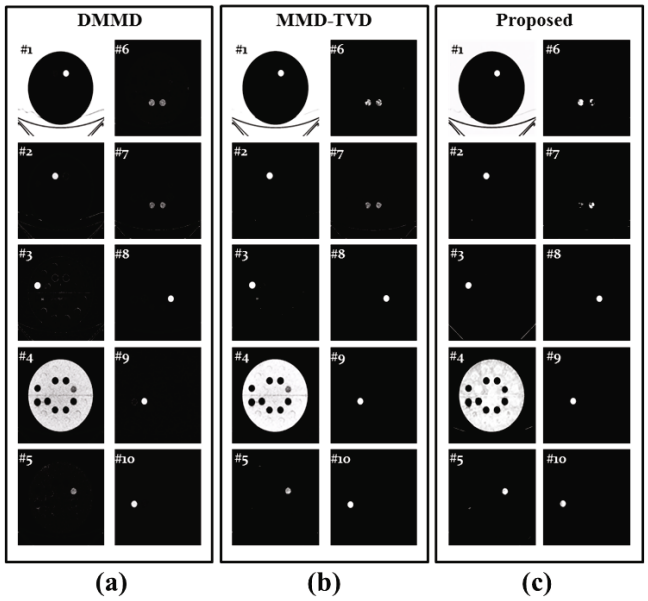

Fig. 7. Decomposed images of the tissue characterization phantom as obtained using (a) the DMMD, (b) the MMD-C, and (c) the proposed methods: LN-300 (#1), LN-450 (#2), adipose (#3), solid water (#4), liver (#5), inner bone (#6), bone mineral (#7), 30% $CaCO_3$ (#8), 50% $CaCO_3$ (#9), and cortical bone (#10).

where x_{lj} is the fraction value of the l-th pixel in the ROI of the j-th material image, and M is the total number of pixels in the selected ROI.

III. RESULTS

To compare the performance of the proposed method, we used the DMMD and the MMD-TVD methods. The MMD-TVD method consists of decomposition and post-decomposition stages. The TVD was applied on decomposed images only during post-processing [13,14,24,25]. For all images in this study, the display window ranged from zero to one.

1. Digital Phantom

We selected fat, water, blood, and air as the basis materials. Figure 5 shows the references and the decomposed images of the digital phantom with noise. For blood images obtained using the DMMD and the MMD-TVD methods, soft tissue material remains. The proposed method clearly acquired blood materials in blood images because this method calculated more proper material triplet for each pixel by reducing the noise before decomposition.

The VFA values of the decomposed basis material images are shown in Fig. 6. Several ROIs (#1, #2, and #3 as shown in Table 2) located within the uniform areas of the basis materials are selected for quantitative analysis. The average values of the VFA were 81.72%, 84.71%, and 93.12% when using the DMMD, the MMD-TVD, and the proposed methods, respectively. These results show that the proposed method achieves improved decomposition accuracy.

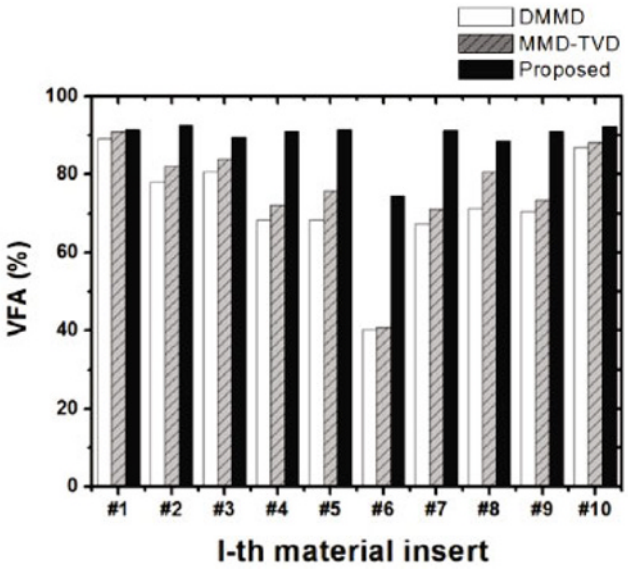

Fig. 8. VFA values of 10 basis material images for the tissue characterization phantom as obtained using the DMMD (white), the MMD-TVD (gray), and the proposed (black) methods.

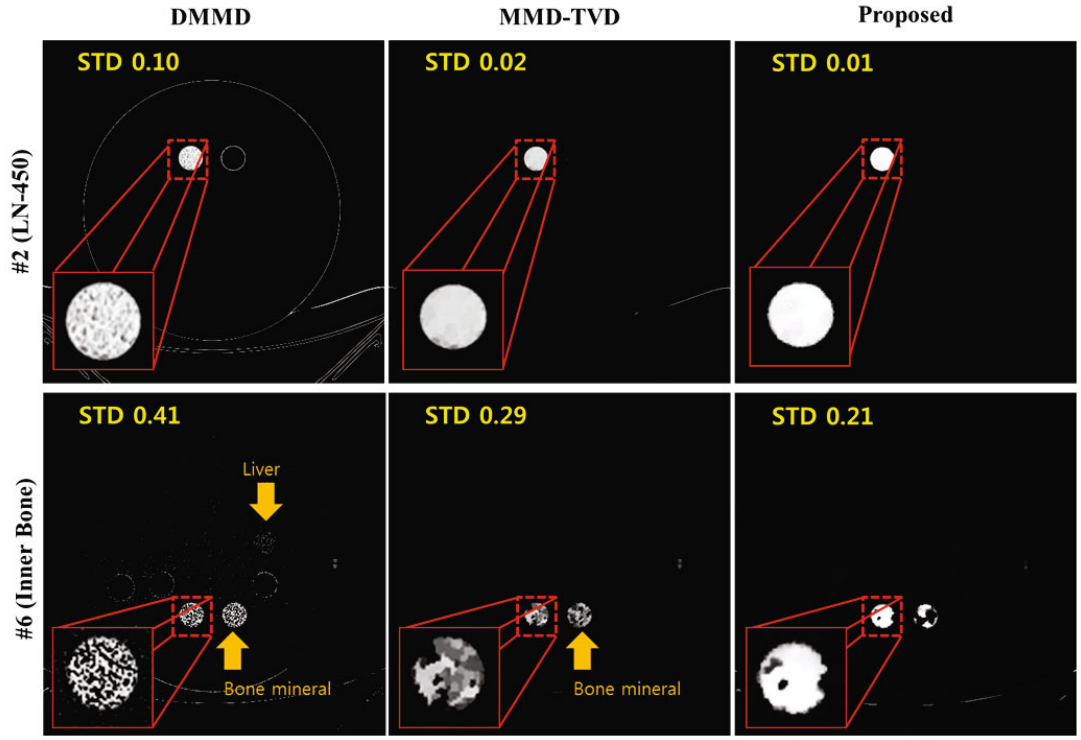

Fig. 9. Decomposed images of the tissue characterization phantom as obtained using the DMMD (1st column), the MMD-TVD (2nd column), and the proposed (3rd column) methods: decomposed LN-450 (the 1st row) and inner bone (4th row) images.

2. Tissue Characterization Model 467 Phantom

We obtained 10 material basis images by using the three algorithms, as shown Fig. 7. Figure 8 shows the calculated VFA values of the decomposed material images. The average VFA values obtained using the DMMD (white), the MMD-TVD (gray), and the proposed method (black) were 76.34%, 79.04%, and 95.47%, respectively. In all ROI values of the decomposed images as basis materials, the proposed method yielded VFA values that were more accurate compared to the DMMD and the MMD-TVD methods. In particular, the proposed method improved the average VFA value of three decomposed images (liver, inner bone, bone mineral) by 37.57% compared with the DMMD method.

Figure 9 shows that LN-450 (the 1st row) and the inner bone (2nd row) images acquired by using the DMMD (1st column), the MMD-TVD (2nd column), and the proposed methods (3rd column). For the three algorithms, the LN-450 images are clearly distinguished from other materials. The VFA values for their images, obtained using the proposed method, were closer to 100% than the values obtained using the other methods. In the inner bone images obtained using the DMMD and the MMD-TVD methods, the small difference in the LAC values between the inner bone and the bone mineral materials is difficult to distinguish because CT images include noise. When the proposed method was used, inner bone images could be distinguished from bone mineral materials.

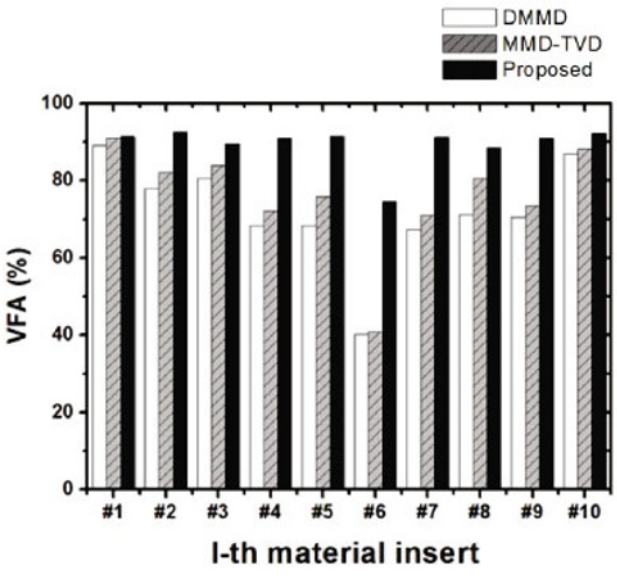

Fig. 10. VFA values of 10 basis material images for the Catphan phantom as obtained using the DMMD (white), the MMD-TVD (gray), and the proposed (black) methods.

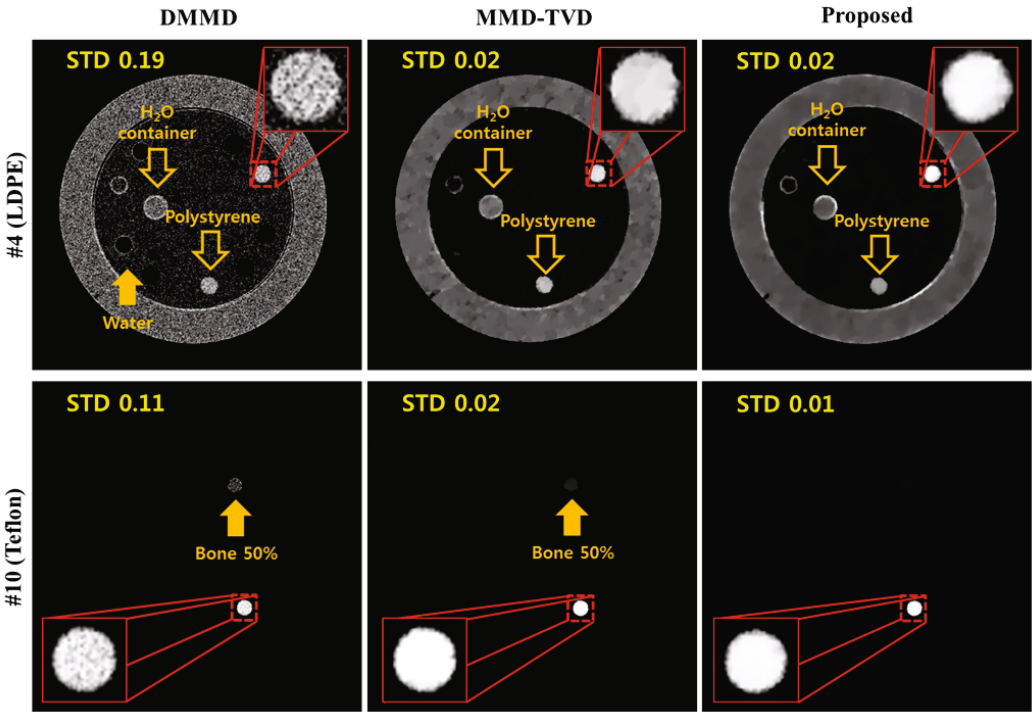

Fig. 11. Decomposed images of the Catphan 700 phantom as obtained using the DMMD (1st column), the MMD-TVD (2nd column), and the proposed (3rd column) methods: decomposed LDPE (1st row) and Teflon (2nd row) images

3. Catphan 700 Phantom

Figure 10 shows the VFA values of the decomposed material images for the Catphan phantom. The total average of VFA values obtained using the DMMD, the MMD-TVD, and the proposed methods were 72.04%, 75.91%, and 89.35%, respectively.

Figure 11 shows that LDPE (the 1st row) and the Teflon (2nd row) images that were acquired by using the DMMD (1st column),the MMD-TVD (2nd column), and the proposed (3rd column) methods. The LDPE images for all three algorithms included the H_2O container and polystyrene materials, because these materials were not the selected basis materials. Bone 50% materials was detected in Teflon images using DMMD and MMD-TVD methods because the differences of LAC values for the two materials was small. However, the proposed method distinguished inner bone images from bone minerals and other materials.

IV. DISCUSSION AND CONCLUSIONS

The proposed MMD framework consists of three steps: pre-decomposition, decomposition, and post-decomposition. The noise suppression algorithm in the pre- and the post-stages suppressed the image quality degradation due to material triplet selection and direct inversion.

We used total variation denoising as the noise suppression algorithm. Total variation denoising is typically considered as a procedure of DECT independent of reconstruction; thus, it is computationally more convenient. In this study, we calculated the maximum VFA value to select the proper values for parameters when we used total variation denoising; however, selecting the proper parameter values is challenging. Further study may be needed to derive the proper values of the parameters [24].

The results of the proposed method were compared to those of the DMMD [11] and the MMD-TVD methods. Compared to the DMMD, the proposed method improved the average VFA by 11.40%, 17.31%, and 19.13% in the digital phantom, the tissue characterization phantom, and the Catphan phantom studies, respectively. The VFA values that obtained using the MMD-TVD method were similar to those values obtained using the DMMD method. This showed that noise suppression after decomposition has limitations for improving the decomposition accuracy. Differentiating between basis materials with small LAC differences by using the DMMD and the MMD-TVD methods was difficult. The results showed that the proposed method more clearly distinguishes basis materials with small density differences. The reason was that our method calculated a more proper material triplet for each pixel by reducing noise before decomposition.

The averaged STDs for the tissue characterization phantom as obtained using the DMMD, the MMD-TVD, and the proposed methods were 0.17, 0.07, and 0.06, re-

spectively. Those for the Catphan phantom were obtained using the DMMD, the MMD-TVD, and the proposed methods were 0.19, 0.03, and 0.02, respectively. The STD values for the proposed method are better than those of the DMMD method, and similar to those of the MMD-TVD method. Thus, the proposed method improves the decomposition accuracy and reduces noise simultaneously. Further study may be needed to apply the proposed method to clinical CT data.

In conclusion, the proposed method can improve the decomposition accuracy by reducing the noise both before and after decomposition. The results show the possibility that the proposed method may be able to provide quantitative improvement for multi-material decomposition in conventional DECT.

REFERENCES

[1] R. K. Kaza *et al.*, RadioGraphics **32**, 353 (2012).
[2] C. H. McCollough, S. Leng, L. Yu and J. G. Fletcher, Radiology **276**, 637 (2015).
[3] M. Patino *et al.*, Radiographics **36**, 1087 (2016).
[4] H. W. Goo and J. M. Goo, Korean J. Radiol. **18**, 555 (2017).
[5] C. Thomas *et al.*, Eur. Radiol. **19**, 1553 (2009).
[6] M. Qu *et al.*, Am. J. Roentgenol. **196**, 1279 (2011).
[7] J. Cloutier, L. Villa, O. Traxer and M. Daudon, World J. Urol. **33**, 157 (2015).
[8] R. F. Barber, E. Y. Sidky, T. G. Schmidt and X. Pan, Phys. Med. Biol. **61**, 3784 (2016).
[9] P. Stenner, T. Berkus and M. Kachelriess, Med. Phys. **34**, 3630 (2007).
[10] Y. Long and J. A. Fessler, IEEE Trans. Med. Imaging **33**, 1614 (2014).
[11] P. R. S. Mendonca, P. Lamb and D. V. Sahani, IEEE Trans. Med. Imaging **33**, 99 (2014).
[12] Y. Xue *et al.*, Med. Phys. **44**, 886 (2017).
[13] Q. Ding, T. Niu, X. Zhang and Y. Long, Med. Phys. **45**, 3614 (2018).
[14] Q. Lyu, D. OConnor, T. Niu and K. Sheng, J. Med. Imaging **6**, 044004 (2019).
[15] Y. Xue *et al.*, IEEE Trans. Comput. Imaging **5**, 515 (2019).
[16] Y. Jiang *et al.*, IEEE Tras. Biomed. Eng. **67**, 523 (2020).
[17] D. S. Rigie, A. A. Sanchez and P. J. L. Riviere, Phys. Med. Biol. **62**, 3284 (2017).
[18] T. Niu, X. Dong, M. Petrongolo and L. Zhu, Med. Phys. **41**, 041901 (2014).
[19] A. Chambolle and T. Pock, J. Math. Imaging Vis. **40**, 120 (2010).
[20] P. O. Persson and G. Strang, SIAM Rev. **46**, 329 (2004).
[21] F. Mirzaei and R. Faghihi, BJR Open **1**, 20180008 (2019).
[22] J. H. Hubbell, S. M. Seltzer, NIST. X-ray Mass Attenuation Coefficients. https://www.nist.gov/pml/x-ray-mass-attenuation-coefficients, last accessed May 22, 2020.
[23] J. Punnoose*et al.*, Med. Phys. **43**, 4711 (2016).
[24] A. K. Carton *et al.*, Br. J. Radiol. **83**, 344 (2010).
[25] D. S. Rigie and P. J. L. Riviere, Phys. Med. Biol. **60**, 1741 (2015).